Ultrasound-assisted rapid growth of water compatible magnetite nanoparticles

A. M. TOMOIAGĂ[a,b], A. VASILE[a], M. ALEXANDROAEI[a], I. SANDU[c,d,*]
[a] *Department of Chemistry, "Alexandru Ioan Cuza" University of Iasi, 11 Carol I Bd., 700506, Iasi, Romania*
[b]*Research Department, ChemPerformance Ltd., 37 Fintinilor Street, 700337, Iasi, Romania*
[c] *Arheoinvest Interdisciplinary Platform, "Alexandru Ioan Cuza" University of Iasi, 11 Carol I Bd., 700506, Iasi, Romania*
[d] *Romanian Inventors Forum, Str. Sf. Petru Movila, no. 3, Bl. L11, III/3, 700089, Iasi, Romania*

Water compatible magnetite nanoparticles have been successfully prepared by ultrasound-assisted reversed chemical precipitation method. This method enables synthesis of gram-scale magnetite nanoparticles in a rapid, low-cost, reproducible and easy-to-handle manner. More, this preparation method is easily scalable to meet industrial requirements. XRD, SEM, FTIR, N_2-sorption and room-temperature VSM are the techniques used to investigate the structural, textural, morphological and magnetic properties of the obtained nanoparticles. The results show that the obtained nanoparticles display superparamagnetic behavior, hidrophillicity, homogeneous particle sizes of ~20 nm and low agglomeration tendency, making them very promising platform for biomedical applications. The factors governing the formation of magnetite nanoparticles by ultrasound-assisted reversed chemical precipitation are discussed extensively.

(Received December 2, 2013; accepted January 22, 2014)

Keywords: Superparamagnetic nanoparticles, Magnetite, Sonochemical synthesis, Hydrophilic magnetic nanoparticles, Iron oxides

1. Introduction

In the last century magnetic materials have become indispensable to daily life, representing ones of the most familiar functional materials intensely used for motors, power distribution systems, and medicine [1]. Among magnetic materials, nanosized magnetite display fascinating properties due to their small size and large surface area, having potential applications in many fields as biomedicine [2-5], biomolecular nanopatterning [6], recyclable nanobiocatalysts [7], biosensors [8], catalysis [9], environmental remediation [10] etc. Magnetite (Fe_3O_4) is a common magnetic iron oxide with cubic inverse spinel structure with oxygen forming a face-centered cubic closed packing and iron cations occupying interstitial tetrahedral sites and octahedral sites [11].

For high performance in function-specific biological applications magnetic nanoparticles should have small sizes (<100 nm) and narrow size distributions, high crystallinity, large surface area (for maximal protein or enzyme binding), good dispersity in water and high magnetic saturation to provide maximum signal. It is very difficult to prepare nanoparticles to meet all the requirements above. Slight modifications of their properties greatly influence the successful application in specific fields. It is well known that magnetic properties strongly depend on the morphologies and size of the nanoparticles, while residual magnetism induces aggregation among the particles. When the particle size is adequately small, each particle is a single magnetic domain and exhibits superparamagnetic property above the blocking temperature [12]. Superparamagnetic nanoparticles quickly respond to the applied external magnetic field, and their remanent magnetization and coercivity are negligible. Accordingly, when superparamagnetic nanoparticles are used in the field of biomedicine, undesirable particle agglomerations originated from the residual magnetism can be avoided. Moreover, water compatibility of these nanoparticles is a must if one intents to use them in biomedical applications. Although hydrophilicity may be induced by adding a transfer agent, with hydrophilic ends, capable, with one end to bind to the particle surface and with the other one to render the particles hydrophilic, the nanoparticles subjected to these treatments often suffer low stability.

Thus, there is an emerging need to develop rapid, easy to handle, cheap and reproducible methods to synthesize magnetic nanoparticles with special features suitable for specific applications in biomedicine. In the last decade, substantial progress in the size control and properties tuning of magnetic nanoparticles to fit target biomedical applications has been made by developing preparation procedures such as co-precipitation [13], thermal decomposition [14], microwave-assisted preparation [15] etc. However, most of the preparation methods either required use of non-hydrolytic solvents [14] or of $Fe2+/Fe^{3+}$ whose co-precipitatiom is more difficult to control [13], or are time consuming [16,17]. Ultrasonic irradiation was reported previously as an effective alternative for the synthesis of magnetic nanoparticles in various conditions [18-21]. Sonochemistry relies on acoustic cavitation phenomena, i.e. the formation, growth

and collapse of bubbles in a liquid medium. The ultrasonic irradiation of liquids produces localized hot spots that can initiate chemical reactions. By controlling cavitation conditions, it is then possible to tailor the chemical reactivity [22-24].

Therein, we report a facile and efficient method to synthesize stable magnetite nanoparticles (NPs) under ultrasonic irradiation, by reversed chemical precipitation. The used reagents are cheap and the fabrication process is one step, requires low temperature, is easy to achieve in short time and open atmosphere. Water compatibility is induced by *in-situ* capping of the nanoparticles surface with citrate molecules, thus attaining high dispersity and increased stability in water. The morphological, structural and textural features, assessed by XRD, SEM, FTIR and VSM make these NPs very versatile for further functionalization and application in various biomedical fields.

2. Materials and methods

2.1 Materials

Fe_3O_4 NPs were prepared using ferrous sulphate heptahydrate ($FeSO_4 \cdot 7H_2O$, 98%) purchased from Aldrich. Sodium hydroxide (NaOH) and sodium nitrate ($NaNO_3$) were received from Merck; trisodium citrate dihydrate ($C_6H_5Na_3O_7 \cdot 2H_2O$, 99%) was acquisitioned from Sigma. All chemicals were used as received without further purification. Deionized water used throughout the experiments was prepared with an ELGA purelab water system.

2.2 Characterization methods

Synthesis of the magnetite nanoparticles was performed by sonicating the solution with an ultrasonic processor SONICS VIBRA Cell^{TM} Model CV 33 which operates at 20kHz and provides a maximum power of 750W. To avoid rapid increase of temperature in the reaction medium, the generated ultrasound is triggered following a cycled periodic pulse. The duration of ultrasound was 3s, and the resting time was 1s. The instrumentation is equipped with a 13mm diameter titanium tip immersed directly in the solution.

Powder X-ray diffraction (XRD) patterns were recorded on Panalytical X'Pert Pro MPD diffractometer employing $Cu_{K\alpha}$ radiation (λ = 0.154nm). Θ–2Θ scans were performed in the 2Θ range 20 – 80° in steps of 0.04°, counting 2s per step. The lattice parameter of the sample (cubic Fd-3m space group) has been calculated by Rietveld refinement using X'Pert HighScore Plus v.2.2.3. The global factors included the scale factor, 2θ zero error correction, Lorentz polarization factor, polynomials of background fitting and crystal linear absorption coefficient were refined. Positions, occupancy factors and overall isotropic displacement parameters of individual atoms of the initial unit cell were fixed during analysis. Bruker Tensor 27 Spectrometer was used for recording FTIR. The samples were measured as KBr diluted pellets. The scans were collected with a resolution of $4cm^{-1}$, over the spectral range 400 – $4000cm^{-1}$. The morphology and particle sizes were observed by Scanning Electron Microscopy (SEM) using a Vega Tescan electron microscope. A few drops of sample dispersion in ethanol were deposited on the sample holder and the solvent evaporated at room temperature. Nitrogen sorption isotherms were performed on a Quantachrome Nova 2200 Instrument & Pore Size Surface Area Analyzer at - 196°C on samples degassed at room temperature for 12h under vacuum, calculating BET specific surface area from the linear part of the plot. Magnetic measurements were performed on a vibrating sample magnetometer (VSM) Princeton Instruments Micromag™ 3600 at room temperature.

3. Experimental

3.1 Preparation of Fe_3O_4 nanoparticles

Water compatible Fe_3O_4 NPs were prepared by a facile one-step precipitation method under ultrasonic irradiation in the presence of trisodium citrate. A typical synthesis of hydrophilic magnetite NPs consists in the following steps: (i) preparation of 2M Fe^{2+} solution by dissolving the necessary amount of $FeSO_4 \cdot 7H_2O$ in 10mL of deionized water; (ii) preparation of a solution containing trisodium citrate (0.05M), sodium nitrate (0.01M) and sodium hydroxide (0.2M) by dissolving proper amounts in 40 mL deionized water and slow heating up to 100°C; (iii) precipitation of Fe^{2+} in alkaline media by fast addition of a proper volume of 2M Fe^{2+} solution into the second solution (equivalent to 0.2M Fe^{2+} in the alkali solution) under ultrasonic irradiation of mixed solution; (iv) formation and growth of Fe_3O_4 nanoparticles under ultrasonic irradiation for 1h (an abundant black precipitate is obtained); (v) cooling down to room temperature naturally; (vi) nanoparticles recovery thorough magnetic decantation; (vii) washing with deionized water several times; (viii) drying at 60°C overnight. All the steps of this synthesis method were performed in open atmosphere.

These Fe_3O_4 nanoparticles can be easily dispersed in water and used as seeds for preparation of advanced drug delivery nanosystems with targeting functions and sustained release properties.

4. Results

4.1 Structural features of Fe_3O_4 hydrophilic nanoparticles

Comparing XRD pattern of synthesized nanoparticles, shown in figure 1, with the standard diffraction pattern (Powder Diffraction Files PDF, Ref. no 19-0629), it is clearly observed that the synthesized product is crystalline Fe_3O_4. The Bragg reflections at 30, 35.2, 43, 54, 57, 63, and 74,9° observed correspond to (220), (311), (400),

(422), (511), (440) and (622) planes of magnetite face-centered cubic spinel structure with space group *Fd3m*. The lattice parameter of the sample (cubic spinel Fd-3m space group) has been calculated by Rietveld refinement using Topas Acdemic v4.1 which implements fundamental parameters approach (FPA). FPA uses a convolution-based profile fitting calculated from the emission profile, instrumental and sample contributions without a reference sample [25]. The obtained value of the lattice parameter is a = 8.341(6)Å. The global factors included the scale factor, 2θ zero error correction, Lorentz polarization factor, polynomials of background fitting and crystal linear absorption coefficient were refined. Positions, occupancy factors and overall isotropic displacement parameters of individual atoms of the reference unit cell (Inorganic Crystal Structure Database Reference Code: 96012) were fixed during analysis.

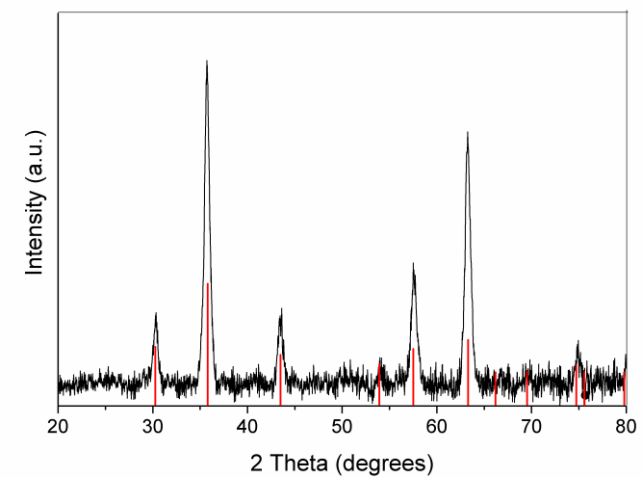

Fig. 1. XRD patterns of sonochemically-developed citrate-capped magnetite NPs. The vertical red lines indicate the Fe3O4 diffractions of the cubic spinel structure, Powder Diffraction Files PDF, Ref. no 19-0629.

Using Scherrer's equation for the more intense diffractions [26], a grain size of 16 nm was calculated for citrate-capped NPs. However, it is well known that calculations for nanoparticle size using Scherrer equation is not reliable, being often affected by errors. Therefore these findings are verified by SEM measurements.

4.2 Surface investigation of water compatible Fe_3O_4 nanoparticles

To understand nature of the surface of Fe_3O_4 NPs, we performed FTIR measurements on citrate-capped NPs and on pure citrate (Fig. 2). In the low wavenumbers region, one intense band occurs at 560cm^{-1} in the FTIR spectra (marked with an arrow) recorded on the Fe_3O_4 NPs. This band is readily assigned to stretching vibrations Fe – O – Fe in magnetite. At higher wavenumbers the FTIR spectra recorded on magnetite NPs resembles with that of the pure citrate. Two intense absorption bands are observed at 1639 cm^{-1} and 1385cm^{-1} which are readily assigned to the stretching vibrations of ν(as, COO^-) and ν(s, COO^-) of citrate molecules [27]. Furthermore, absorption bands characteristic to ν(as, - CH_2 -) and ν(s, - CH_2 -) from citrate molecules are present at 2925cm^{-1} and 2850cm^{-1}, in the FTIR spectra recorded on sonochemically-developed magnetite NPs. These results indicate that the citrate molecules have been linked on the surface of the nanoparticles being part of these nanoparticles.

The broad IR adsorption band at 3100 – 3500cm^{-1} is generally assigned to water molecules adsorbed on the surface, proving the presence of water molecules on the surface of sonochemically-developed magnetite nanoparticles. Therefore, we proceeded to the assessment of surface hidrophilicity by means of water adsorption in static conditions for 24h. The amount of absorbed water was established using Karl-Fisher titration and proven to be of 23.53% for these sonochemically developed Fe_3O_4 NPs, confirming their water compatibility.

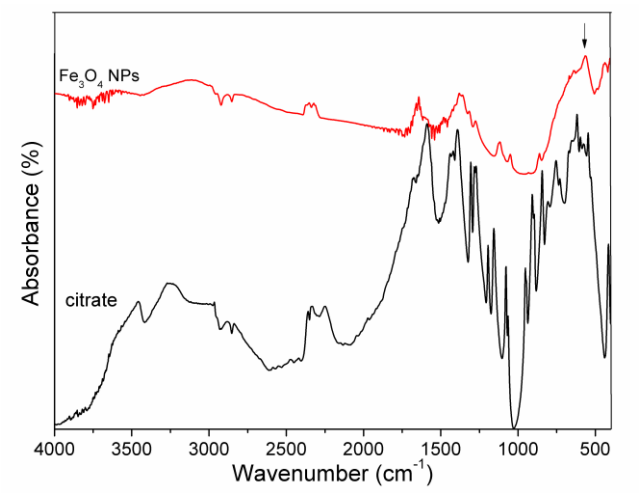

Fig. 2. FTIR spectra of pure citrate and of citrate-capped Fe_3O_4 NPs prepared by ultrasonic reversed chemical precipitation.

Fig. 3 shows the N_2-sorption isotherm recorded on sonochemically-developed magnetite nanoparticles. The sample display a type II isotherm in IUPAC classification, characteristic to non-porous materials, with a narrow hysteresis loop at high values of relative pressures (P/P_0 = 0.85 – 0.98). This hysteresis occurs due to the micropores formed between nanoparticles (interparticles porosity). Specific surface area of Fe_3O_4 NPs prepared in sonochemical conditions was calculated to be of 100m^2/g, using BET equation on the linear part of the adsorption isotherm (P/P_0 = 0.053 – 0.260)

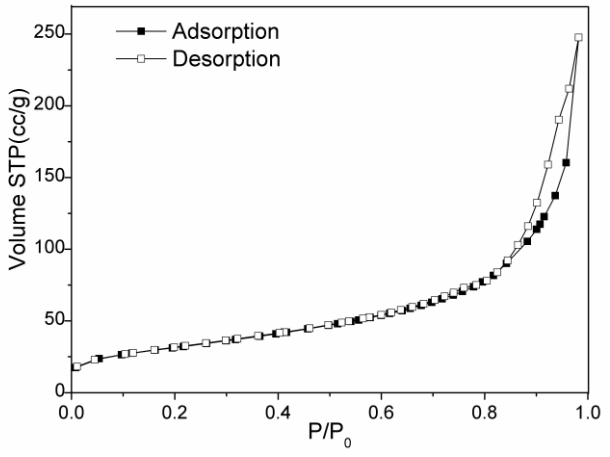

Fig. 3. N_2 adsorption-desorption isotherm recorded on sonochemically-developed citrate-capped magnetite NPs.

4.3 Morphology of the water compatible Fe_3O_4 nanoparticles

Scanning Electron Microscopy (SEM) was used to observe nanoparticles morphology and uniformity of particle sized. Recorded micrographs are presented in Fig. 4. It is clearly observed that the nanoparticles are spherical, with homogeneous size distribution. The average particle size is estimated to be ~ 20nm and their tendency to agglomerate is low, due to the presence of citrate molecules capped on their surface.

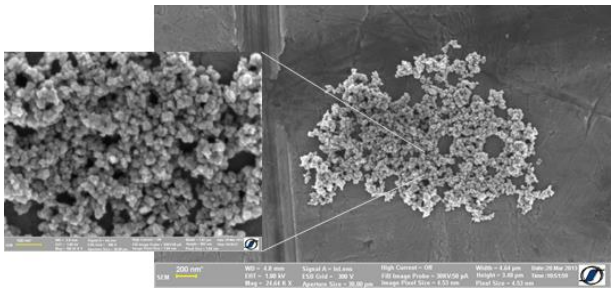

Fig. 4. SEM Images of sonochemically-developed citrate-capped magnetite NPs.

4.4 Magnetic properties of the water compatible Fe_3O_4 nanoparticles

To investigate the magnetic properties of sonochemically-prepared magnetite nanoparticles, measurements were carried out in an applied magnetic field at room temperature. The field dependence of isothermal magnetization measured is shown in figure 5. The measured saturation magnetization (Ms) and coercive field (Hc) values were found to be of 51emu/g and 23Oe, while the remanent magnetization was found to be of 2.5emu/g. On the basis of the criteria given by Dunlop et al. [28], the value of Mr/M_S should be larger than 0.5 for single-domain (SD) particles, between 0.1 and 0.5 for pseudosingle domain (PSD) particles and lower than 0.1 for multidomain (MD) particles. The sonochemically prepared magnetite nanoparticles show an MD-type behavior ($Mr/Ms < 0.1$). These data and the steep magnetization curves are related to finite-size and surface effects, thus the prepared Fe_3O_4 NPs are considered to be superparamagnetic, meaning that the thermal energy can overcome the anisotropy energy barrier of a single particle.

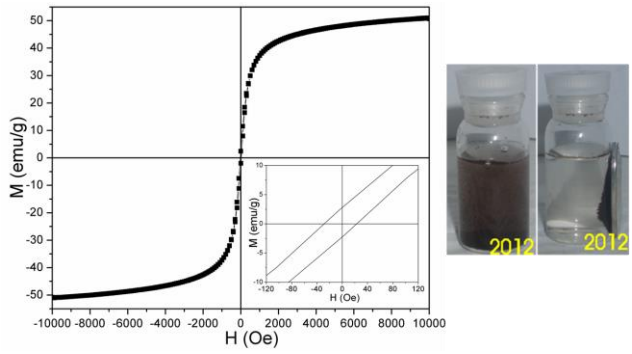

Fig. 5. Magnetization curves of sonochemically-developed citrate-capped magnetite NPs.

5. Discussions

The size, dispersity and stability in water, are important issues when considering magnetic nanoparticles for biomedical applications. As a general rule, the average diameter of magnetite NPs strongly depends on the Ostwald Ripening process. The key to control sizes of the nanoparticles is to tune the competition between nucleation and growth. When growth rate of seeds exceeds the nucleation rate, larger nanoparticles will be formed. Olowe and Genin concluded that in the synthesis of magnetite starting only from ferrous ions, formation of $Fe(OH)_2$ is the first reaction to take place and Fe_3O_4 is obtained as a result of dehydration reaction of ferrous hydroxide and ferric hydroxide, the latter compound being produced by the partial oxidation of ferrous hydroxide by the oxygen dissolved in water [29]. These authors have proposed the following mechanism for the formation of magnetite starting only from ferrous salts:

$$Fe^{2+} + 2HO^- \rightarrow Fe(OH)_2$$
$$3Fe(OH)_2 + 1/2O_2 \rightarrow Fe(OH)_2 \cdot 2FeOOH + H_2O$$
$$Fe(OH)_2 \cdot 2FeOOH \rightarrow Fe_3O_4 + 2H_2O$$

where $Fe(OH)_2 \cdot 2FeOOH$ is the intermediate compound called hydrated magnetite. There are many factors governing the control the growth over nucleation process. One is reverse precipitation which refers to the addition of acidic ferrous solution to a large amount of basic solution in order to have a better control over the pH value of reaction medium so that all the components precipitate completely as hydroxides, allowing homogenous co-precipitation to occur within individual droplets [20, 24]. It

was previously demonstrated that smaller nanoparticles are formed, in sonochemical conditions, by reverse precipitation than by oxidation of $Fe(OH)_2$ obtained by addition of alkaline solution to aqueous ferrous solution [23, 24].

Another key factor governing the formation of magnetic nanoparticles is the oxidation rate of $Fe(OH)_2$. As stated before aqueous $FeSO_4$ can react with NaOH to yield $Fe(OH)_2$ which is readily converted to $Fe(OH)_3$ by oxidation with dissolved oxygen in an alkaline medium. When the oxidation of $Fe(OH)_2$ takes place under air, magnetite with a small amount of FeOOH is mainly produced [24]. As the oxidation rate of $Fe(OH)_2$ is increased, the size of the magnetite would decrease significantly. Because the amount of dissolved oxygen in water decreases with increasing temperature, the oxidation rate of $Fe(OH)_2$ is smaller, thus pure-phase magnetite products will be obtained at more elevated temperatures [20, 27]. Therefore we have firstly heated our alkaline solution up to 100°C and then subjected to ultrasound irradiation in ambiental conditions. It is well known that he implosive collapse of bubbles generates extremely high temperature (~5000K), high local pressure (about 20MPa), and heating - cooling rates above 10^{10}K/s [22, 30]. Thus, at the end of the synthesis process, the final solution containing Fe_3O_4 nanoparticles was still hot and cooled down to room temperature naturally.

In our work nanosized magnetite nanoparticles with average sizes of 20nm were obtained under ultrasonic irradiation by reverse chemical precipitation. On the other hand, when similar synthesis was performed under magnetic stirring, larger nanoparticles with average sizes of ~ 35 nm were obtained (data not shown). This can be easily explained by the effective agitation and in situ formation of active species via cavitational collapse when the reaction solution is subjected to ultrasonic wave action [19, 20]. In the solution subjected to ultrasonic irradiation, water molecules are thermally decomposed to generate hydrogen atom and hydroxyl radical, which can recombine to form dihydrogen, hydrogen peroxide, and water [19]. Higher amounts of hydrogen peroxide would be thus formed when oxygen or air is dissolved in water [24]. The magnetite nanoparticles would be produced through the oxidation of $Fe(OH)_2$ by hydrogen peroxide. Thus, the formation rate of magnetite nuclei under ultrasonic irradiation was accelerated when compared with that under magnetic stirring [19].

The size of magnetite nanoparticles is also affected by the ionic strength of the reaction medium. Hui and colab. [27] reported that 20nm Fe_3O_4 nanoparticles are readily formed through reverse chemical precipitation in 10M $NaNO_3$, while 40-nm nanoparticles can be formed without $NaNO_3$. Moreover, these authors show that the increase of ionic strength using anions enhances the distribution of the charges of the nanoparticles surrounded with citric acid radical [27]. Thus, the charge of the citrate ions plays a key role on the dispersity and stability of the magnetic nanoparticles in water because the repulsive forces between the electrical charges of citrate radical ions make nanoparticles to be more dispersed in water. We have explored the stability of sonochemically prepared magnetite nanoparticles in water, and find out that they are stable for several weeks.

5. Conclusions

Water compatible citrate-capped Fe_3O_4 nanoparticles have been successfully synthesized in one step by ultrasonic reversed chemical precipitation, avoiding deoxygenated conditions and Fe^{2+}/Fe^{3+} molar ratio control. The proposed method is easy reproducible and suitable for preparation of Fe_3O_4 nanoparticles on gram scale using cheap reagents, low temperature and short reaction time. The prepared nanoparticles are stable in water, have uniform particle sizes of ~20 nm and display superparamagnetic behavior. These features make them very attractable for further functionalization and applications in biomedicine. Therefore, presently we are using these citrate-caped magnetite nanoparticles as seeds in the formation of core-shell magnetic mesoporous silica composites in order to use them as nanocarriers for targeted delivery of low-molecular antineoplastic drugs.

Acknowledgements

This work was financially supported by the European Special Found in Romania, under the responsibility of the Managing Authority for the POSDRU 2007-2013, project – POSDRU/89/1.5/S/63663 (COMMSCIE).

References

[1] N. Spaldin, Magnetic Materials: Fundamentals and Device Applications, Cambridge University Press, Cambridge, 2003.
[2] O. S. Nielsen, M. Horsman, J. Overgaad, Eur. J. Cancer, **37**, 1587 (2001).
[3] P. Tartaj, M. P. Morales, T. González-Carreño, S. Veintemillas-Verdaguer, C. J. Serna, J. Magn. Magn. Mater., **28**, 290 (2005).
[4] L. C. Varanda, M. Jafelicci Junior, W. Beck Junior, in LASKOVSKI, A. N. (Ed.), Biomedical Engineering, Trends in Materials Science, 2011, p. 397.
[5] M. M. Yallapu, S. F. Othman, E. T. Curtis, B. Gupta, M. Jaggi, S.C. Chauhan, Biomat, **32**, 1890 (2011).
[6] Z. Gu, S. X. Huang, Y. Chen, Angew. Chem. Int., Ed. **48**, 952 (2009).
[7] W. Wang, Y. Xu, D. I. C. Wang, Z. Li, J. Am. Chem. Soc., **131**, 12892 (2009).
[8] H. Ben Fredj, S. Helali, C. Esseghaier, L. Vonna, L., Vidal, A. Abdelghani, Talanta, **75**, 740 (2008).
[9] S. Shylesh, V. Schünemann, W. R. Thiel, Angew. Chem. Int. Ed., **49**, 3428 (2010).
[10] S. Rakshit, D. Sarkar, E. J. Elzinga, P. Punamiya, R. Datta, J. Haz. Mater., **221**, 246 (2013).
[11] R. M. Cornell, U. Schwertmann, The Iron Oxides: Structure, Properties, Reactions, Occurrence and Uses,

Wiley-VCH: New York, 2nd edition, 2003, p. 32.
[12] A.-H. Lu, E. L. Salabas, F. Schüth, Angew. Chem. Int. Ed., **46**, 1222 (2007).
[13] M. Ma, Y. Zhang, W. Yu, H.Y. Shen, H.Q. Zhang, N. Gu, Coll. Surf. A **212**, 219 (2003).
[14] F. Zhao, N. Zhang, L. Feng, Mater Lett., **68**, 112 (2012).
[15] F. Miao, W. Hua, L. Hu, K. Huang, Mater. Lett., **65**, 1031 (2011).
[16] S. Sun, H. Zeng, S. Raoux, D. B. Robinson, S. X. Wang, P. M. Rice, G. Li, J. Am. Chem. Soc. **126**, 273 (2004).
[17] W. D. Zhang, H. M. Miao, L. P. Zhu, S. Y. Fu, J. Alloys Compd., **477**, 736 (2009).
[18] G. Marchegiani, P. Imperatori, A. Mari, L. Pilloni, A. Chiollerio, P. Allia, P. Tiberto, L. Suber, Ultrason Sonochem, **19**, 877 (2012).
[19] F. Dang, N. Enomoto, J. Hojo, K. Enpuku, Ultrason Sonochem., **16**, 649 (2009).
[20] J. P. Cheng, R. Ma, D. Shi, F. Liu, X.B. Zhang, Ultrason Sonochem., **18**, 1038 (2011).
[21] S. Wu, F. Zhai, J. Wang, W. Xu, Q. Zhang, A.A. Volinsky, Mater Lett., **65**, 1882 (2011).
[22] K. S. Suslick, Y. Didenko, M. M. Fang, T. Hyeon, K. J. Kolbeck, W.B. McNamara III, M.M. Mdleleni, M. Wong, Philos. Trans. R. Soc., Lond., A, **357**, 335 (1999).
[23] T. Shuto, Y. Mizukoshi, S. Tanabe, H. Kurokawa, IEICE Trans. Fund. Electron. Commun. Comp. Sci., **J89**-A, 729 (2006).
[24] Y. Mizukoshi, T. Shuto, N. Masahashi, S.J. Tanabe, Ultrason. Sonochem., **16**, 525 (2009).
[25] R. W. Cheary, A. A. Coelho, Journal of Applied Crystallography, **25**, 109 (1992).
[26] F. Yazdani, M. Edrissi, Mater. Sci. Eng., B, **171**, 86 (2010).
[27] C. Hui, C. Shen, T. Yang, L. Bao, J. Tian, H. Ding, C. Li, H.-J. Gao, J. Phys. Chem., C., **112**, 11336 (2008).
[28] D. J. Dunlop, Rep. Prog. Phys., **53**, 707 (1990).
[29] A. A. Olowe, J.M.R. Genin, Corr. Sci., **32**, 965 1991.
[30] F. Dang, N. Enomoto, J. Hojo, K. Enpuku, Ultrason. Sonochem., **17**, 193 (2010).

*Corresponding author: ion.sandu@uaic.ro